Quantitative analysis of the angular dynamics of a single spheroid in simple shear flow at moderate Reynolds numbers

Tomas Rosén,[1,2,*] Arne Nordmark,[1] Cyrus K. Aidun,[3] Minh Do-Quang,[1] and Fredrik Lundell[1,2]

[1] *KTH Mechanics, Royal Institute of Technology, SE-100 44 Stockholm, Sweden*

[2] *Wallenberg Wood Science Center, Royal Institute of Technology, SE-100 44 Stockholm, Sweden*

[3] *G. W. Woodruff School of Mechanical Engineering and Parker H. Petit Institute for Bioengineering and Bioscience, Georgia Institute of Technology, Atlanta, Georgia 30332-0405, USA*

(Received 16 February 2016; published 1 August 2016)

A spheroidal particle in simple shear flow shows surprisingly complicated angular dynamics; caused by effects of fluid inertia (characterized by the particle Reynolds number Re_p) and particle inertia (characterized by the Stokes number St). Understanding this behavior can provide important fundamental knowledge of suspension flows with spheroidal particles. Up to now only qualitative analysis has been available at moderate Re_p. Rigorous analytical methods apply only to very small Re_p and numerical results lack accuracy due to the difficulty in treating the moving boundary of the particle. Here we show that the dynamics of the rotational motion of a prolate spheroidal particle in a linear shear flow can be quantitatively analyzed through the eigenvalues of the log-rolling particle (particle aligned with vorticity). This analysis provides an accurate description of stable rotational states in terms of Re_p, St, and particle aspect ratio (r_p). Furthermore we find that the effect on the orientational dynamics from fluid inertia can be modeled with a Duffing-Van der Pol oscillator. This opens up the possibility of developing a reduced-order model that takes into account effects from both fluid and particle inertia.

DOI: 10.1103/PhysRevFluids.1.044201

I. INTRODUCTION

The study of particles in fluid flows has attracted a lot of attention during the last century due to the vast applicability in describing industrial [1–3], biological [4–6], and geophysical processes [7–9]. In order to be able to pinpoint the important physical processes, numerical simulations have been growing to become a crucial scientific tool to complement the traditional experimental approaches. The straightforward way of simulating these flow problems is through direct numerical simulations, where the coupled motions of fluid and particle are simultaneously calculated. However, this quickly becomes computationally expensive as the number of particles increase, since the numerical grid resolution must be very fine around each particle for accurate results. If the particles are small, and if the concentration of particles is low, the forces exerted by the particles on the fluid can be neglected. This enables the use of Lagrangian Particle Tracking (LPT) methods. In LPT the particle trajectories are defined by local forces and their orientational dynamics are evaluated in the linearized reference frame of each particle. Generally many of these systems have been modeled with spherical particles due to the availability of models for the hydrodynamic force and torque [10]. However, for a large number of cases, the nonsphericity of the particles is crucial for the suspension properties such as rheology, mixing, and particle interactions. Jeffery [11] derived analytical expressions for the torque on ellipsoidal particles in linear flow fields, which enables LPT to be applied to nonspherical particles [12]. However, these methods are restricted by the assumption that neither the particle nor the fluid around the particle has any inertia. Particle inertia can be included in such models by allowing acceleration terms to be active in the particle equations of motion [13–15], but the influence of fluid inertia is more difficult to characterize as the flow field changes significantly around the

*rosen@mech.kth.se

particle [16–18]. In conclusion, it is desirable to find a model of the orientational dynamics for a single, nonspherical, particle that takes into account both fluid and particle inertia. This can then be used in a Lagrangian frame in a fluid simulation.

To tackle this problem, some assumptions must be made with respect to the practical flow problem that we want to describe: (1) The suspension is assumed to be dilute and particles are not interacting with each other either hydrodynamically or through collisions. (2) Any influence of turbulence is neglected as this can cause small-scale fluctuations of the flow field around the particle and also local concentration variations that might violate the first assumption [15,19,20]. (3) The translational velocity of each particle is the same as the local fluid velocity, which implies that sedimentation is neglected and the flow is stationary with straight streamlines. If there is no such slip velocity between particle and fluid, any translational drift of particles to neighboring streamlines cannot occur because Saffman and Magnus forces are not present; this assumption also implies that the Lagrangian frame around each particle is an inertial frame of reference following the fluid. (4) The particles are assumed to be large enough for Brownian diffusion to be neglected. (5) The particles have rotational symmetry and potential chaotic motions due to triaxiality is neglected [21–23]. (6) The flow field inside the Lagrangian frame is assumed to be a linear shear flow, i.e., there are no second spatial derivatives of the flow velocity. With these assumptions, the study of a single spheroidal particle in a simple shear flow provides fundamental knowledge to understand the orientational dynamics of nonspherical particles in fluid flows. Although these assumptions render the flow problem highly idealized, understanding the physics in this system can still provide a strong foundation that will make it possible to tackle each one of the assumptions. It should be noted, however, that the results presented in the paper are not based on these assumptions, and the only assumptions made are based on DNS of governing equations.

In this work, we consider the aforementioned flow problem with numerical simulations and provide the first accurate and domain-size independent results at moderate Re_p. We also isolate the respective effects from fluid and particle inertia. Specifically we find that the fluid-inertia effects lead to orientational dynamics similar to that of a Duffing-Van der Pol oscillator. These results are important steps towards a reduced-order model for both fluid and particle inertia to be used in LPT methods. We concentrate on describing the prolate spheroid but also briefly comment on the case of an oblate spheroid.

A. Formulation of the problem

A single prolate spheroid with density ρ_p is rotating in a simple shear flow, which is created by the motion of two parallel walls separated by distance L and moving in opposite directions with velocity U, as shown in Fig. 1(a). The coordinate frame is centered on the particle center of mass, and the particle orientation is determined by a unit vector along the particle symmetry axis ($\boldsymbol{s}$). The particle has an aspect ratio, r_p, defined by the ratio between the symmetry axis length and the equatorial diameter. A prolate spheroid thus fulfills $r_p > 1$ and an oblate spheroid $r_p < 1$. The motion of the fluid with density ρ_f and kinematic viscosity ν is governed by the incompressible Navier-Stokes equations. The equations are nondimensionalized using: the particle major axis l (which is the same as symmetry axis length for a prolate spheroid) as characteristic length, the inverse shear rate $[G^{-1} = L/(2U)]$ as a characteristic time, and $\rho_f \nu G$ as a characteristic pressure. With these scalings, the nondimensional equations read

$$\nabla \cdot \boldsymbol{u} = 0,$$
$$\mathrm{Re}_p\left[\frac{\partial \boldsymbol{u}}{\partial t} + (\boldsymbol{u} \cdot \nabla)\boldsymbol{u}\right] = -\nabla p + \nabla^2 \boldsymbol{u} + \boldsymbol{f}. \tag{1}$$

These describe the evolution of the fluid velocity $\boldsymbol{u}$ and pressure p when being subject to volumetric forces $\boldsymbol{f}$, where the size of the inertial term is governed by the particle Reynolds number defined as $\mathrm{Re}_p = Gl^2/\nu$. The confinement of the system is defined as $\kappa = l/L$. Through the no-slip condition at the particle surface ($\boldsymbol{u} = \boldsymbol{\omega} \times \boldsymbol{r}$, with particle angular velocity $\boldsymbol{\omega}$ and $\boldsymbol{r}$ as a position vector to the

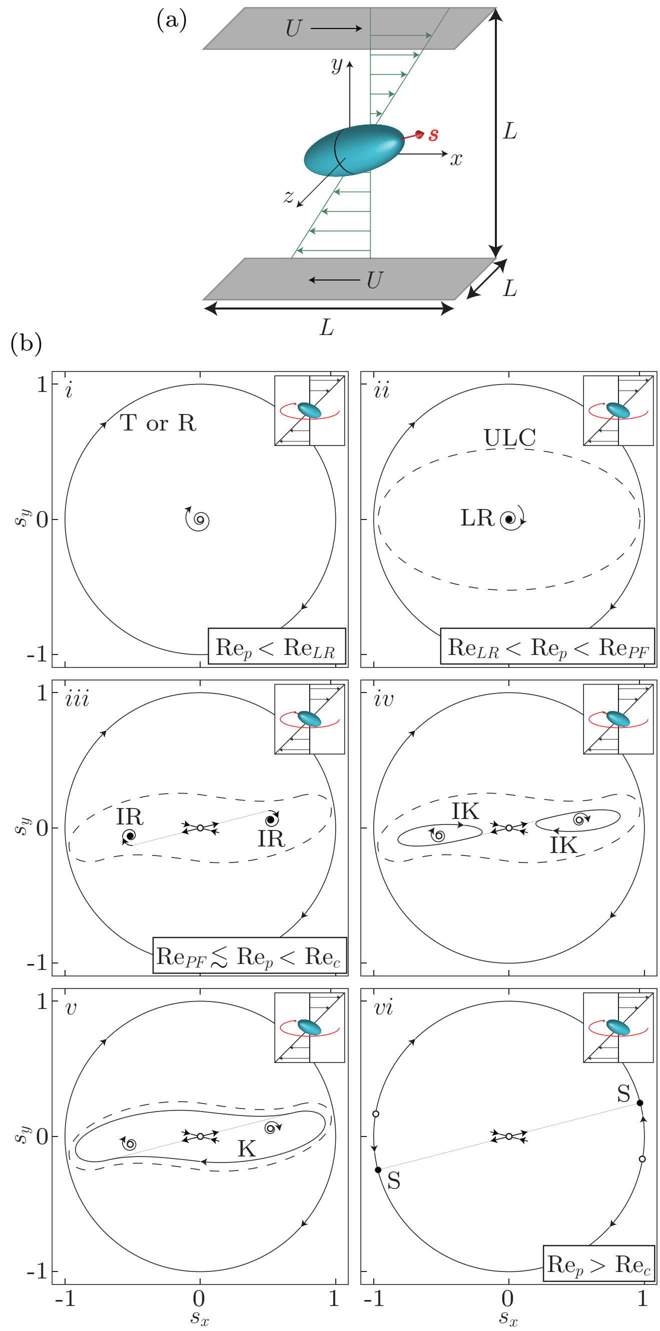

FIG. 1. (a) Illustration of the flow problem of a single prolate spheroidal particle in a linear shear flow; (b) stable rotational states illustrated by the trajectory of (s_x, s_y) in different parameter regions i–vi; (i) planar rotation of tumbling (T) or rotating (R); (ii) planar rotation and log rolling (LR); (iii) planar rotation and inclined rolling (IR); (iv) planar rotation and inclined kayaking (IK); (v) planar rotation and kayaking (K); (vi) steady state (S); the planar states (T and R) and nonplanar states (LR, IR, IK, and K) are separated by an unstable limit cycle (ULC).

particle surface; both quantities nondimensional), the fluid enforces stresses on the surface giving a resulting (nondimensional) torque $\boldsymbol{M}$, from which the particle rotation is determined through the nondimensional equation of motion:

$$\boldsymbol{M} = \mathrm{St}[\boldsymbol{I}\dot{\boldsymbol{\omega}} + \boldsymbol{\omega} \times (\boldsymbol{I}\boldsymbol{\omega})], \tag{2}$$

where $\boldsymbol{I}$ is the (nondimensional) inertial tensor of the spheroid. The additional scalings required to nondimensionalize the second equation are the characteristic torque ($\rho_f \nu G l^3$) and the characteristic inertial tensor element ($\rho_p l^5$). The size of the particle inertial term in the equation is governed by the Stokes number $\mathrm{St} = \alpha \mathrm{Re}_p$ where $\alpha = \rho_p/\rho_f$ is the solid-to-fluid density ratio. The reaction forces from the particle on the fluid are in turn included in the force term in Eq. (1).

B. Summary of previous work

The pioneering work in Ref. [11] provided a complete description of the motion of an unconfined ($\kappa = 0$) ellipsoidal particle in any linear flow in the absence of inertia, i.e., $\mathrm{St} = \mathrm{Re}_p = 0$. However, in this degenerate case, no preferential rotational state exists for a prolate spheroid in a simple shear flow, and the rotation depends on the initial orientation. It was shown by Bretherton [30] that the same angular dynamics of the spheroid can be described with the vector $\boldsymbol{q}$, where

$$\dot{\boldsymbol{q}} = \begin{pmatrix} 0 & \frac{1}{2}(\varepsilon + 1) & 0 \\ \frac{1}{2}(\varepsilon - 1) & 0 & 0 \\ 0 & 0 & 0 \end{pmatrix} \boldsymbol{q}, \tag{3}$$

with

$$\varepsilon = \frac{r_p^2 - 1}{r_p^2 + 1}.$$

The dynamics of the particle symmetry axis can then easily be obtained by disallowing the deformation of the vector through the normalization $\boldsymbol{s} = \boldsymbol{q}/|\boldsymbol{q}|$, which ensures that unit length is maintained.

Lundell and Carlsson [31] used the torque ($\boldsymbol{M}$) on a spheroid in creeping shear flow in Ref. [11] and coupled this to the equation of motion [Eq. (2)]. In this way the dynamics at $\mathrm{Re}_p = 0$ (but finite $\mathrm{St} > 0$) was obtained. Particle inertia was found to cause a drift of the prolate spheroid towards rotation in the flow-gradient plane ($s_z = 0$) due to centrifugal forces.

The final *planar* dynamics can be described with the evolution of the angle ϕ, defined as the angle between the symmetry axis $\boldsymbol{s}$ and the x axis. According to Nilsen and Andersson [32], the planar dynamics is described by the following:

$$\frac{St}{80}\Lambda(K_1 + \Lambda K_2)\ddot{\phi} = \varepsilon\left(\frac{1}{2} - \cos^2\phi\right) + \frac{1}{2} - \dot{\phi}, \tag{4}$$

where

$$\Lambda = \frac{1-\varepsilon}{1+\varepsilon},$$

$$K_1 = \int_0^\infty \frac{d\beta}{(1+\beta)^{3/2}\left(r_p^{-2} + \beta\right)},$$

$$K_2 = \int_0^\infty \frac{d\beta}{\sqrt{1+\beta}\left(r_p^{-2} + \beta\right)^2}.$$

At $\mathrm{St} = 0$, the particle will rotate with a period as described by in Ref. [11]: $T_J = 2\pi(r_p + r_p^{-1})$ in an intermittent rotation called *tumbling*. As $\mathrm{St} \to \infty$, particle inertia becomes much greater than the viscous forces from the fluid, and the particle will rotate with constant angular velocity along with the local vorticity, i.e., with a period $T_H = 4\pi$ (subscript H for *heavy*). This type of motion is called *rotating*. Lundell and Carlsson [31] defined a transitional Stokes number ($\mathrm{St}_{0.5}^*$) where the period is $T = (T_J + T_H)/2$ and particle inertia is of the same order of magnitude as viscous forces. With the corrections from Ref. [32], this number is found to be

$$\mathrm{St}_{0.5}^* = \frac{80[0.7 + 0.3[1 - \varepsilon^2]^{5/8})]}{\Lambda[K_1 + \Lambda K_2]}. \tag{5}$$

Although influence from particle inertia is quite well understood, the influence from fluid inertia at $\mathrm{Re}_p \neq 0$ is more complicated to describe. Several experimental [33–36], theoretical [37–39], and direct numerical [24–28,40] methods have been used to address the problem. Although preferential rotational states were found as a consequence of fluid and particle inertia, a complete, fundamental, understanding of the motion remains elusive due to contradicting results.

In order to distinguish the effects of particle and fluid inertia respectively, St and Re_p need to be studied independently from each other. In any practical case, in order to fulfill the assumptions in Sec. I, St must equal to Re_p in order for no sedimentation to occur in the presence of gravity. However, by studying the dynamic behavior in the case of $\mathrm{St} \neq \mathrm{Re}_p$, we can both predict what happens for neutrally buoyant particles ($\alpha = 1$) and gain valuable insights for the development of a reduced-order model of the system.

Rosén *et al.* [29] performed direct numerical simulations of the flow problem at $\kappa = 0.2$, with variations in Re_p, St, and particle aspect ratio (r_p). The found rotational states are summarized in Fig. 1(b), which schematically draws the flow-gradient (xy) components of the orientation vector (s_x, s_y). At low Re_p, it was found that the particle drifts towards *planar* rotation of *tumbling* ($s_z = 0$ and ω_z varies with orientation) or *rotating* ($s_z = 0$ and ω_z is almost constant) and is represented by the circular trajectory in Fig. 1(b) i–v. At higher Re_p, the stable planar rotation can coexist with a stable *nonplanar* state with $s_z \neq 0$ [Fig. 1(b) ii–v]. At a certain $\mathrm{Re}_p = \mathrm{Re}_{LR}$, the *log-rolling* state ($s_x = s_y = 0$) stabilizes in a subcritical Hopf bifurcation [Fig. 1(b) ii]. In this bifurcation, an unstable limit cycle (ULC) is created and determines which initial conditions that lead to planar or nonplanar motion, respectively. The log-rolling state is destabilized at $\mathrm{Re}_p = \mathrm{Re}_{PF} > \mathrm{Re}_{LR}$, in a supercritical pitchfork bifurcation creating two symmetrical fixed points corresponding to the *inclined rolling* state at $(s_x, s_y) = (A, B)$ and $(s_x, s_y) = (-A, -B)$, where A and B are positive nonzero constants [Fig. 1(b) iii]. Further increasing Re_p, we get *inclined kayaking* [Fig. 1(b) iv] and *kayaking* [Fig. 1(b) v], and above a certain $\mathrm{Re}_p \geqslant \mathrm{Re}_c$, the particle can assume a stationary *steady state* [16] where $s_z = \omega_z = 0$ [Fig. 1(b) vi]. As long as $r_p \gtrsim 3$, the dynamics was found to follow the same sequence of bifurcations when increasing Re_p at $\alpha = 1$. However, for neutrally buoyant spheroids with low aspect ratio ($r_p \leqslant 2$), the period doubled and chaotic orbits were found at $\mathrm{Re}_{PF} < \mathrm{Re}_p < \mathrm{Re}_c$ in Refs. [26,29].

Although these results were found to be qualitatively unaffected by numerical grid resolution, it was not possible to obtain the precise quantitative transitional numbers. This would require a stability analysis, otherwise the required spatial resolution and excessive time integration becomes computationally intractable. This is also believed to be one of the reasons for previous numerical studies being quantitatively inconsistent. Another reason is that the confinement is seen to influence the results significantly at $\kappa > 0.2$, and most of the previous studies have insufficiently sized domains for the results to be domain-size independent. In other cases, the particle is initialized in an orientation far away from a stable solution, and it is thus difficult to distinguish when the bifurcations occur. A summary of the transitions between rotational states found in previous numerical works at moderate Re_p is presented in Table I. It is clear that there remains no general quantitative description of this flow problem.

Recently, the works by Einarsson *et al.* [41,42] and Candelier *et al.* [43] provided a complete theory for the orientational dynamics of a spheroid in an unconfined ($\kappa = 0$), linear shear flow at infinitesimal Re_p that was consistent with observations from numerical simulations. To assess the validity of these results, Rosén *et al.* [44] performed a numerical linear stability analysis of the log-rolling spheroid and confirmed the quantitative values of the stability exponent provided

TABLE I. Inconsistencies in some of the previous numerical studies of a neutrally buoyant ($\mathrm{St} = \mathrm{Re}_p$) prolate spheroid in simple shear flow at moderate Re_p; the simulations by Mao and Alexeev [28] were performed in a triply periodic domain using Lees-Edwards boundary conditions in the velocity gradient direction and using density ratio $\alpha = 0.1$ ($\mathrm{St} = \mathrm{Re}_p/10$) when studying the three-dimensional rotation.

Previous work	κ	Re_{LR} ($\alpha = 1$)	Re_{PF}	Re_c	Remarks
Qi and Luo [24]	0.5	205–345 ($r_p = 2$)	–	–	Few initial orientations and high κ
Yu *et al.* [25]	0.4	$\lesssim$128 ($r_p = 2$)	224–256 ($r_p = 2$)	–	Few initial orientations and high κ
Huang *et al.* [26]	0.5	120 ($r_p = 2$)	235 ($r_p = 2$)	445 ($r_p = 2$)	High κ
Huang *et al.* [27]	<0.2	–	–	167 ($r_p = 3.3$) 120 ($r_p = 5$)	Did not compute stability of states
Mao and Alexeev [28]	<0.2*	$\lesssim$50 ($r_p = 2$) $\approx$40 ($r_p = 5$)	–	–	Did not compute stability of states, and few initial orientations
Rosén *et al.* [29]	0.2	23.5 ($r_p = 4$) $\approx$25 ($r_p = 5$)	155.5 ($r_p = 2$) 61.5 ($r_p = 4$) 60.5 ($r_p = 5$)	103 ($r_p = 3.3$) 90 ($r_p = 4$) 89 ($r_p = 5$)	Not converged in terms of grid resolution

in Refs. [41,42] as $\mathrm{Re}_p,\kappa \to 0$. In Ref. [44] we also find the required corrections in terms of Re_p and κ for the theory to be applicable for small Re_p and confined systems. However, the theory was not sufficient to explain the complicated dynamics seen for moderate Re_p ($\mathrm{Re}_p \gtrsim 1$) in previous numerical work, e.g., Ref. [26].

As mentioned in Ref. [40], the important dynamical transitions at Re_{LR} and Re_{PF} are explained by the linear stability of the log-rolling spheroid. It was further argued that the sequence of bifurcations might originate from the fact that the log-rolling state is close to having a double zero eigenvalue for a certain choice of parameters. By utilizing the same linear stability analysis as Ref. [44], which is already seen to be consistent with theory when $\mathrm{Re}_p,\kappa \to 0$, we will address this hypothesis. We will also study much higher values of St than Ref. [29] did previously, to find the full appearance of the state space that is applicable as $\mathrm{St} \to \infty$. Consequently, in this work, we combine the qualitative direct numerical simulations with the quantitative linear stability analysis and can finally provide a complete and accurate theory of the prolate spheroid in simple shear flow.

C. The Duffing-Van der Pol oscillator

Rosén *et al.* [40] found that the sequence of bifurcations seen between nonplanar states, as Re_p increases, was very similar to a typical dynamical system: a Duffing-Van der Pol (DVP) oscillator [45,46]. This system describes a one-dimensional inertial system:

$$\ddot{x} = (\mu_1 - x^2)x + (\mu_2 + x^2)\dot{x}, \tag{6}$$

where μ_1 and μ_2 are constants. This system has odd symmetry around the origin, with nonlinear restoring forces and nonlinear damping. Following the idea in Ref. [30], we study the x and y components of a vector ($\boldsymbol{q}$) that has similar dynamics to the symmetry axis ($\boldsymbol{s}$) but is free to deform, i.e., $\boldsymbol{s} = \boldsymbol{q}/|\boldsymbol{q}|$. We then use the DVP oscillator to describe the qualitative noninertial two-dimensional dynamics of q_x and q_y:

$$\begin{aligned}\dot{q}_x &= q_y,\\ \dot{q}_y &= \left(\mu_1 - q_x^2\right)q_x + \left(\mu_2 + q_x^2\right)q_y.\end{aligned} \tag{7}$$

Rewriting it like this, we note that the origin, $q_x = q_y = 0$, corresponds to the log-rolling state, which always is an equilibrium point of the dynamical system. The stability of this equilibrium is

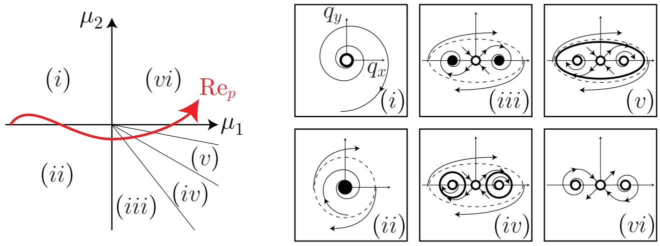

FIG. 2. Dynamical behavior of the DVP oscillator described by Eq. (7) depending on the choice of μ_1 and μ_2; the dynamical behavior is also what we expect in a dynamical system with odd symmetry around the origin (corresponding to the log-rolling state) if this equilibrium point is close to having a double zero eigenvalue; the regions i–vi are analogous to the regions in Fig. 1 when increasing Re_p.

given by the eigenvalues:

$$\lambda_{1,2} = \frac{\mu_2}{2} \pm \sqrt{\frac{\mu_2^2}{4} + \mu_1}. \tag{8}$$

With the choice of $\mu_1 = \mu_2 = 0$, the system thus has a double zero eigenvalue at the origin. Varying the values of these constants, one obtains the different dynamical states illustrated in Fig. 2. The system shows significant similarities to the prolate spheroid in the shear flow. For example, the bifurcation at $\mu_1 < 0$ and $\mu_2 = 0$ corresponds to $\mathrm{Re}_p = \mathrm{Re}_{LR}$, and the bifurcation at $\mu_1 = 0$ and $\mu_2 < 0$ corresponds to $\mathrm{Re}_p = \mathrm{Re}_{PF}$. The behavior of the DVP oscillator is also typical for any nonlinear dynamical system with odd symmetry close to a double zero eigenvalue at the origin [47]. It is not fully known why the infinite dimensional problem of the prolate spheroid in a shear flow behaves like the DVP oscillator, but it must be the cause of symmetry and degeneracy in the system. The odd symmetry around the log-rolling state is easily understood from the nature of the flow problem, but the degeneracy is more difficult to explain. Here we will show that the degeneracy is only caused by fluid inertia at $\mathrm{Re}_p = \mathrm{Re}_{PF}$ where the log-rolling state is close to having a double zero eigenvalue in the absence of particle inertia.

The fact that the angular dynamics of the spheroid in simple shear flow behaves like this simple DVP oscillator in the absence of particle inertia opens up the possibility of finding a reduced-order model to mimic fluid inertial effects at any Re_p. It must be emphasized that the model in Eq. (7) is by no means a good model itself for general particle dynamics, but used only as a demonstrative tool to explain the underlying dynamics in the *nonplanar* motion where $s_z \neq 0$. For example, the model cannot capture the steady-state transition without ensuring that $\dot{q}_y > 0$ at $q_y = 0$ for all $q_x > 0$ at high Re_p. In the present form this is not possible due to the q_x^3 term. However, we hypothesize that, with appropriate modifications of the torque expressions of Ref. [11], we could obtain a dynamical system similar to that of a DVP oscillator.

II. NUMERICAL METHODS

Two numerical methods are used in the present work to approach the current flow problem. First, we perform transient direct numerical simulations (DNS) of the particle motion using the lattice Boltzmann (LB) method [48,49] with external boundary force (LB-EBF [50]). The same method was used by Rosén *et al.* [29,40,44,51]. Second, a linear stability analysis (LSA) of the equilibrium state is performed using the commercial finite-element software Comsol Multiphysics v. 5.1 [52]. In Comsol, we utilize the eigenvalue solver, which is based on ARPACK FORTRAN routines for large eigenvalue problems [52,53]. In this example, the linear stability of the steady state version of Eqs. (1) and (2) is examined for the log-rolling case to capture the critical Re_p and St. The transient motion close to this state can furthermore be analyzed with the same model to observe the influence of the modes corresponding to the leading eigenvalues. Note that all the time-dependent quantities in the results are nondimensionalized using the shear rate, G.

A. Direct numerical simulations (DNS)

In the DNS, the flow problem is set up according to Fig. 1(a), in a cubic domain with $L = 120$ lattice units (l.u.) in each spatial direction. The shear rate is set to be the same as used in Refs. [29,40], i.e., $G = 2U/L = 1/600$ (given in inverse time steps). Periodic boundary conditions are applied in the x and z directions. A prolate spheroid is placed in the middle of the domain and has length $l = 24$ (l.u.) and $r_p = 4$. The confinement is thus constant: $\kappa = 0.2$. The particle is always initialized at rest with initial orientation $\boldsymbol{s} = (\sin 1^\circ, 0, \cos 1^\circ)$, i.e., close to being aligned with the z direction. The particle is then free to rotate until it is judged to have reached the final rotational state, but never longer than $t = 10\,000$ (time scaled with shear rate as mentioned above).

B. Linear stability analysis (LSA)

In the LSA, the flow problem is setup in a cubic domain with the same confinement (κ) as the DNS. The particle was aligned in the vorticity direction $\boldsymbol{s} = (0,0,1)$. Exactly the same method was previously applied in Ref. [44] at low Re_p. The fluid is discretized with a tetrahedral mesh that is free to deform with local grid refinement around the particle. Velocity boundary conditions are applied on the particle surface to ensure that there is no deformation of the grid due to the rotation around the particle symmetry axis. The angular velocity of the particle around the symmetry axis $\omega_z = \omega_S$ is recovered through finding a stationary solution of the governing Eqs. (1) and (2) with $\boldsymbol{s}$ fixed in the z direction. The discretized system is then linearized around this solution to find the most unstable eigenvalues that govern the dynamics close to the log-rolling state. The model provides the N eigenvalues closest to a shift (σ) in the complex plane. In this study we chose $N = 200$ and $\sigma = i\Omega_J$, where $\Omega_J = (r_p^{-1} + r_p)^{-1}$ is the analytical rotational frequency at $\mathrm{Re}_p = St = \kappa = 0$ given in Ref. [11]. The LSA provides us with the list of N eigenvalues $(\lambda_1, \lambda_2, \dots, \lambda_N)$ of the log-rolling particle, ordered by descending real part, i.e., $\Re\lambda_1 > \Re\lambda_2 > \cdots > \Re\lambda_N$. The most unstable eigenvalue λ_1 will determine the dynamics close to the log-rolling state as long as $|\Re\lambda_1| \ll |\Re\lambda_{2\ldots N}|$ and $\Re\lambda_{2\ldots N} < 0$, i.e., all other modes die out quickly.

The solver, with a deformable grid, can also be used to numerically integrate the transient motion close to the log-rolling state ($s_z \approx 1$). This allows us to directly verify the influence of the dominating modes. The transient motion is analyzed by initializing the system in a stationary solution to the particle orientation $\boldsymbol{s} = (\sin 1^\circ, 0, \cos 1^\circ)$.

III. RESULTS

A. DNS

The results from the DNS are summarized in Fig. 3 for a particle of $r_p = 4$, which shows regions in the parameter space with different stable rotational states. Note that the numerical method and lattice Boltzmann parameters used here are the same as in Ref. [29]. The results between these two works are thus directly comparable. However, since much higher Stokes numbers (St) are studied here than in previous work, only the results at $\mathrm{St} \lesssim 1000$ are identical to the results of Ref. [29]. The curve separating the region with only steady state (VIIa) and the region with coexisting tumbling and steady state (VIIb) is called St_c and was taken from Ref. [29]. This is also the case for the curve separating the regions of tumbling (Ia–IVa, VIIb) and rotating states (Ib–IVb, V, VI, VIIc) called $\mathrm{St}_{0.5}$. As mentioned in Sec. I B, this number corresponds to the St where the tumbling period is $T = (T_J + T_H)/2$ and describes when particle inertia is of the same order of magnitude as the viscous damping from the fluid during the planar rotation. The value of $\mathrm{St}_{0.5}$ at $\mathrm{Re}_p = 0$, called $\mathrm{St}^*_{0.5}$, is found through the analytical expressions given by Eq. (5). The final rotational state of the particle initialized close to log rolling is denoted by the symbols.

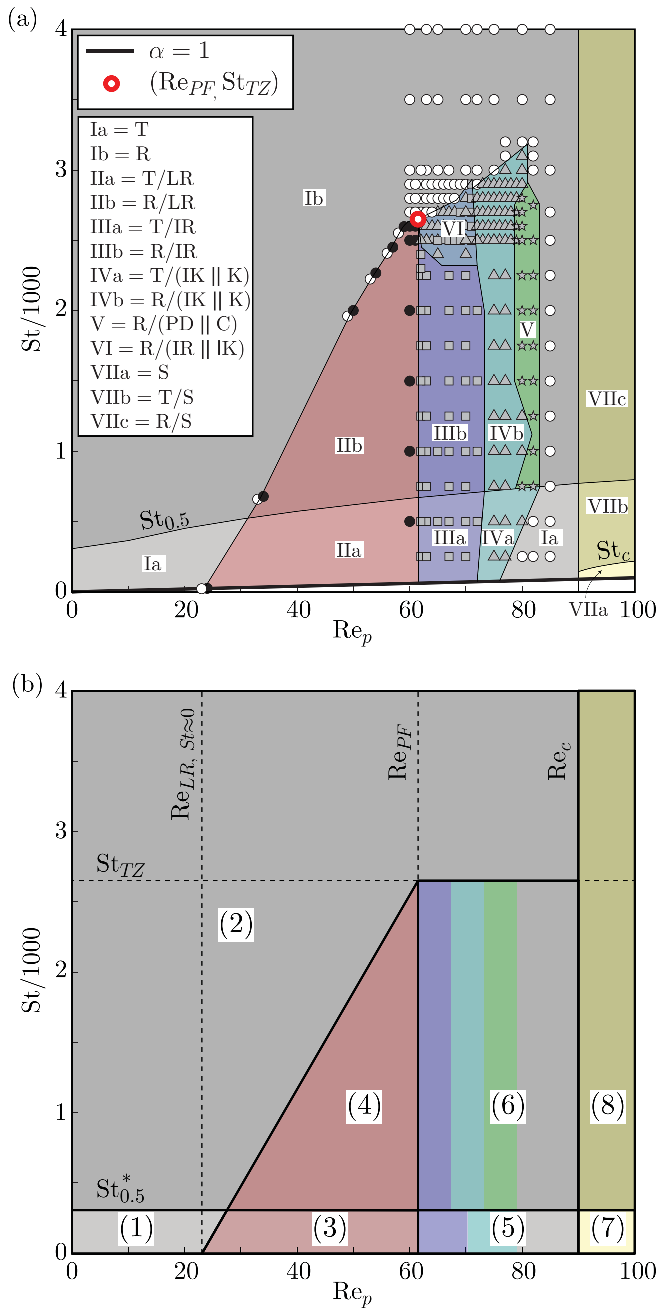

FIG. 3. (a) Results from the direct numerical simulations for a particle with $r_p = 4$ ($\kappa = 0.2$), with the symbols denoting the final state of the particle initialized close to log rolling; T = tumbling and R = rotating (white circles); LR = log rolling (black circles); IR = inclined rolling (gray squares); IK = inclined kayaking and K = kayaking (gray triangles); PD = period-doubled kayaking and C = chaotic kayaking (gray stars); S = steady state. (b) Simplified topology of the state-space using the critical values Re_{PF}, $\mathrm{Re}_{LR,\mathrm{St}\approx 0}$, Re_c, $\mathrm{St}^*_{0.5}$, and St_{TZ}; the stable rotational states in the respective regions 1–8 are described in Table II.

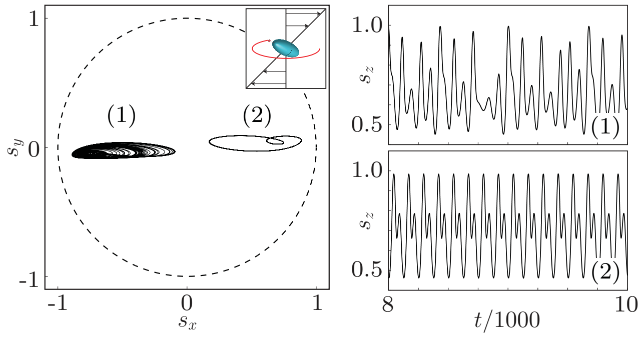

FIG. 4. Trajectories from the DNS at $\mathrm{Re}_p = 80$ for a particle with $r_p = 4$; (1) chaotic kayaking at $\mathrm{St} = 2000$; (2) period-doubled kayaking at $\mathrm{St} = 2500$.

There are two new important features of this state-space topology that were not observed in Ref. [29]. First, the curves Re_{LR} and Re_{PF} separating the region of stable log rolling coincide at a point at $\mathrm{Re}_p = \mathrm{Re}_{PF} = 61.5 \pm 0.5$ and $\mathrm{St} = \mathrm{St}_{TZ} = 2650 \pm 50$ [indicated with the red circle in Fig. 3(a)]. This critical Stokes number thus (in principle) sets a maximum level where nonplanar states can be stable, since more particle inertia will eventually favor the planar rotation. Second, complicated nonplanar dynamics is found in region V (cf. Fig. 3) and illustrated in Fig. 4. In this region we find that states of chaotic kayaking (Fig. 4, case 1) and period-doubled kayaking (Fig. 4, case 2) exist and are long-term solutions to the flow problem. The requirement for having chaotic and period-doubled states seems to be that $\mathrm{St} > \mathrm{St}_{0.5}$, which is a similar requirement for chaotic motion of the prolate spheroid in oscillating shear at $\mathrm{Re}_p = 0$ (reported by Nilsen and Andersson [32]). As mentioned, the transition at $\mathrm{St}_{0.5}$ describes where inertial forces from the particle dynamics are of the same magnitude as the external forces from the fluid. However, this is not a sharp transition, but $\mathrm{St}_{0.5}$ is rather describing the midpoint of a smooth transition in terms of St. Far below this curve, particle inertia is negligible for the nonplanar dynamics, and the particle consequently behaves like a DVP oscillator.

For nonplanar motion, the particle inertial effects enable the type of complicated dynamics seen in Fig. 4. In planar motion, particle inertia controls the transition between tumbling and rotating states. The latter transition is actually similar to St_c, above which nonplanar rotation can coexist with a steady state. All three examples are really describing transitions from noninertial particle dynamics (second derivatives of $\boldsymbol{s}$ are negligible) to inertial particle dynamics where the final rotational state depends on both initial orientation and angular velocity. Even though they occur at slightly different St, the analytical value of $\mathrm{St}^*_{0.5}$ can be seen as a valuable estimate of all these three transitions. With this assumption, we can use only five critical numbers to draw the simplified topology of the state space as done in Fig. 3(b): Re_{PF}, $\mathrm{Re}_{LR,\mathrm{St}\approx 0}$, Re_c, $\mathrm{St}^*_{0.5}$, and St_{TZ}. The different regions of rotational states in Fig. 3(b) are summarized in Table II.

Just as in Ref. [29], the grid resolution in the DNS is not sufficient to provide any quantitatively accurate results. Therefore, only the qualitative dynamics and the topology of the state space can be studied with the resolution employed here. To demonstrate the dependence on the resolution, we find that the critical values of Re_{PF} and St_{TZ} using $L = 240$ ($l = 48$) and $G = 1/1200$ are found at $\mathrm{Re}_{PF} = 75 \pm 5$ and $\mathrm{St} = \mathrm{St}_{TZ} = 2000 \pm 250$. The uncertainties arise as a result of being unable to simulate for long enough to determine if the final state was tumbling, log rolling, or inclined rolling, close to the critical point.

We will show that the critical numbers for drawing the simplified topology can be obtained with high accuracy and without dependence of the numerical domain size, despite these DNS resolution issues.

TABLE II. Stable rotational states in the different regions in Fig. 3(b); T = tumbling; R = rotating; LR = log rolling; IR = inclined rolling; IK = inclined kayaking; K = kayaking; PD = period-doubled kayaking; C = chaotic kayaking; S = steady state.

Region	Planar state	Nonplanar state
1	T	–
2	R	–
3	T	LR
4	R	LR
5	T	IR, IK, or K
6	T	IR, IK, K, PD, or C
7	S	–
8	R or S	–

B. LSA (St = Re_p)

For the LSA, we first consider the case of a neutrally buoyant spheroid (St = Re_p). The real part of the most unstable eigenvalues $\Re\lambda_{1\ldots N}$ are plotted versus Re_p in Fig. 5. At low Re_p, we find that the dynamics close to the log-rolling state is governed by a complex pair of eigenvalues. This was previously investigated in Ref. [44]. We will denote these eigenvalues λ_p (red circles in Fig. 5). At high Re_p, we find that the dynamics is dominated by an unstable real eigenvalue. This eigenvalue is denoted λ_f (blue squares in Fig. 5).

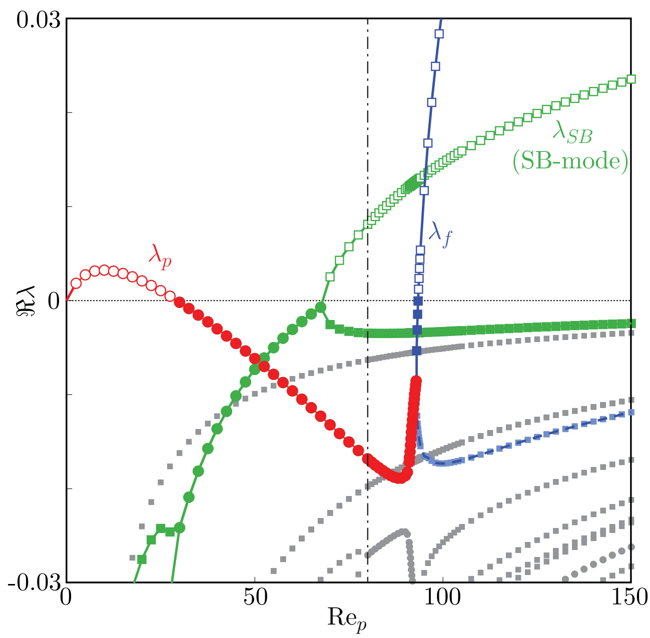

FIG. 5. $\Re\lambda_{1\ldots N}$ as a function of Re_p for a neutrally buoyant particle of $r_p = 4$ (St = Re_p); eigenvalues can be either complex (circles) or real (squares) and be stable (filled symbols) or unstable (open symbols); red symbols show the eigenvalues λ_p, blue symbols denote λ_f, green symbols denote the eigenvalues of the symmetry breaking (SB) mode, and gray symbols are other stable modes which are considered not to influence the dynamics; the dash-dotted line show $\mathrm{Re}_p = 80$, at which the results in Fig. 6 are illustrated.

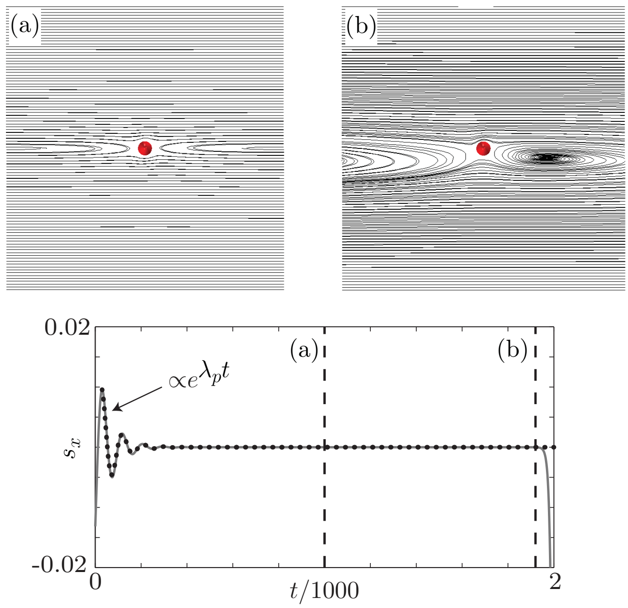

FIG. 6. Flow field showing the influence of the symmetry breaking (SB) mode at $\mathrm{Re}_p = 80$ for a neutrally buoyant particle of $r_p = 4$ at (a) $t = 1000$ and (b) $t = 1920$; the lower plot shows the evolution of s_x compared with the evolution as described by λ_p (dotted).

Apart from these eigenvalues, we observe that there is another eigenvalue (denoted λ_{SB}) that becomes unstable at $\mathrm{Re}_p = 68.75 \pm 1.25$. To observe the influence of the corresponding dynamical mode, we numerically determined the motion at $\mathrm{Re}_p = 80$ where this mode should be dominating. The time series of s_x is shown in Fig. 6. It is clear that the dynamics is initially controlled by the complex eigenvalue λ_p, which takes the particle to a stable log-rolling state ($s_z = 1$). After spending a long time in the log-rolling state, some instability grows in the flow field, where the symmetry is eventually broken (cf. Fig. 6) and the particle moves away from the log-rolling state. Such growth of a global mode, after a long period in a seemingly steady state, has previously been observed in flows without particles, e.g., in a co-flowing wake in Ref. [54]. Furthermore, it is found that the eigenvalues (λ_{SB}) of this symmetry breaking (SB) mode are almost completely unaffected by St. If we assume that the initial disturbance triggering this instability is a small numerical fluctuation in the fluid simulation rather than the particle motion, it should have an initial amplitude on the order of machine precision $\epsilon_0 = O(10^{-16})$. Assuming, furthermore, that it needs to grow to $\epsilon = \epsilon_0 \exp(\lambda_{SB} t) = O(1)$ for it to be present, it would take $t = O(1000)$ until we could see the effect, which is exactly what we observe in Fig. 6. These results indicate that the particle dynamics actually do not inject any energy into the unstable SB mode, and that oscillations of the symmetry axis $\boldsymbol{s}$ stabilize this mode. Since this work is focusing on the orientational dynamics of the spheroidal particle, we discard this mode as a fluid instability, which is interesting to study, but lies outside the scope of the present work.

Following the branch of λ_p in Fig. 5 with increasing Re_p, we find two interesting transitions. The first one is when the complex pair goes from unstable ($\Re\lambda_p > 0$) to stable ($\Re\lambda_p < 0$) at $\mathrm{Re}_p = 28.75 \pm 1.25$. This corresponds to the stabilization of the log-rolling state through the Hopf bifurcation at $\mathrm{Re}_p = \mathrm{Re}_{LR}$, as seen in the DNS. The second one is when $\Im\lambda_p = 0$ and the complex pair is split up into two real eigenvalues at $\mathrm{Re}_p = 92.9 \pm 0.1$. Here the system is close to having the hypothesized double zero eigenvalue. The most unstable real eigenvalue created in this transition is λ_f, as previously introduced.

At slightly higher $\mathrm{Re}_p = 93.4 \pm 0.1$, λ_f becomes unstable, which results in the creation of the inclined rolling state through a pitchfork bifurcation at $\mathrm{Re}_p = \mathrm{Re}_{PF}$, as seen in the DNS. Note that

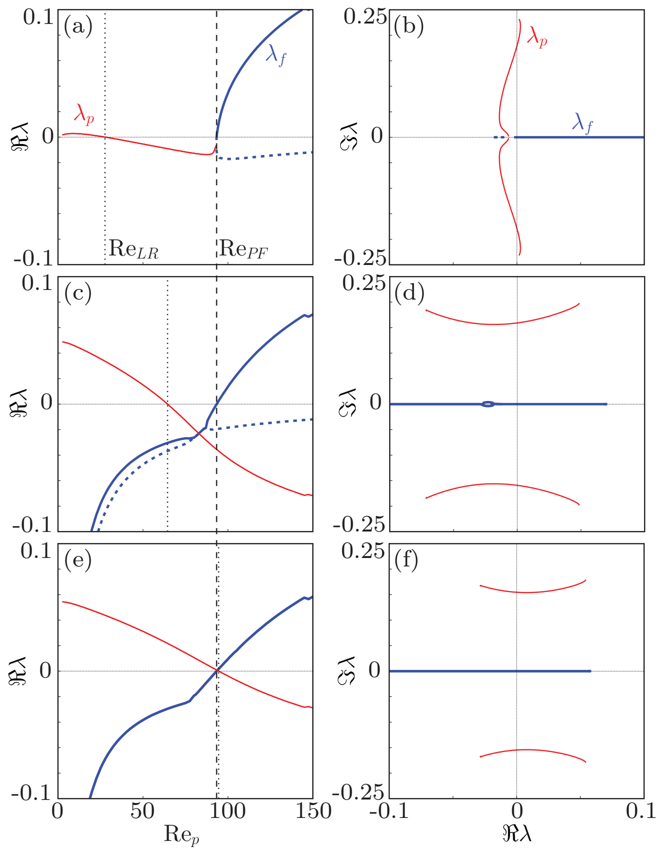

FIG. 7. $\Re\lambda_p$ (thin red line) and $\Re\lambda_f$ (thick blue line) as functions of Re_p for a particle of $r_p = 4$ at three different St; the right figures (b), (d), (e) show the corresponding spectra in the complex plane; (a), (b) St = 1; (c), (d) St = 1500; (e), (f) St = 2000.

this transition implies a transition between two stationary solutions of the flow field and is therefore independent of particle inertia.

The results from this stability analysis, including the fact that the system is close to having a double zero eigenvalue for certain parameters, explains the sequence of bifurcations for the nonplanar rotation seen for the neutrally buoyant particle in Ref. [40].

C. LSA ($\mathrm{Re}_p \neq \mathrm{St}$)

To be able to distinguish between effects from fluid and particle inertia on the dynamics, we performed the same analysis for several other St. We find that there are three distinct regions in terms of St, which are illustrated in Fig. 7. These regions are similar as the ones found in the DNS:

(1) St $< 625 \pm 125$ [illustrated in Figs. 7(a) and 7(b) at St = 1]. Fluid inertia dominates the dynamics; λ_p and λ_f almost connect at the origin in the complex plane at $\mathrm{Re}_p = \mathrm{Re}_{PF}$. At low Re_p ($\mathrm{Re}_p \lesssim \mathrm{Re}_{LR}$), λ_p is unstable even though particle inertia is negligible. This shows that fluid inertia actually causes a drift to planar tumbling in this regime. This falsifies the hypotheses in Refs. [29,31,40], which argued that particle inertia is the dominant cause for this drift (which is of course true at higher St). The fact that fluid inertia is causing a drift towards tumbling at low Re_p was also recently found in Refs. [28,41,42].

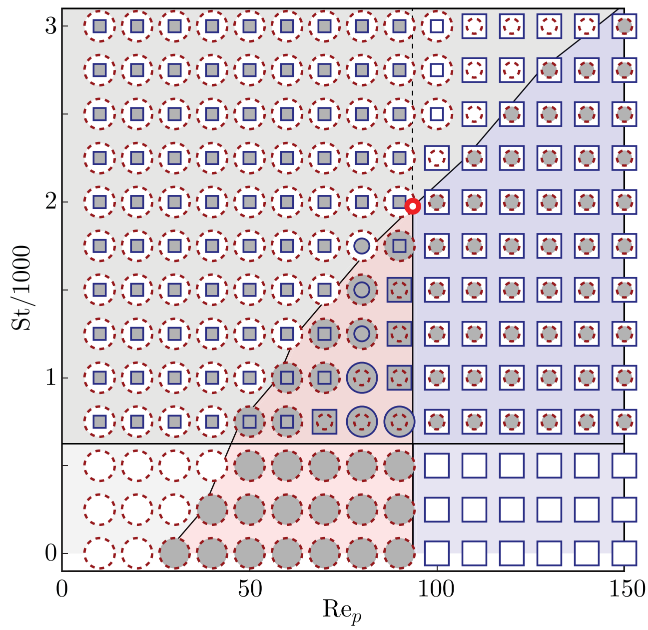

FIG. 8. Stability of the two modes determined by λ_p (symbols with dashed border) and λ_f (symbols with solid border), which control the nonplanar orientational dynamics of the prolate spheroid of $r_p = 4$ as function of Re_p and St; the eigenvalue with larger real part is denoted with a larger symbol; the eigenvalues are either stable (filled symbols) or unstable (open symbols); the parameter pair (Re_{PF},St_{TZ}) is denoted with the thick red circle.

(2) $625 \pm 125 < \mathrm{St} < 1975 \pm 25$ [illustrated in Figs. 7(c) and 7(d) at St = 1500]. Particle and fluid inertia are in competition; λ_p and λ_f are detached and linked to two separate modes, which are present for all Re_p. In the low Re_p regime ($\mathrm{Re}_p \lesssim \mathrm{Re}_{LR}$), λ_p still dominates the dynamics, but at higher Re_p, both modes (three eigenvalues) can be important. At the transition at St = 625 ± 125, the dynamics close to the log-rolling state goes from being two-dimensional (governed by two eigenvalues) to three-dimensional (governed by three eigenvalues), which would explain the complicated dynamics illustrated in Fig. 4.

(3) $\mathrm{St} > 1975 \pm 25$ [illustrated in Figs. 7(e) and 7(f) at St = 2000]. Particle inertia dominates the dynamics; in the Re_p regime where the oscillatory mode of λ_p dominates the dynamics, it is always unstable. At these values of St, log rolling will never be a stable rotational state. Note that at $\mathrm{St} = 1975 \pm 25$ and $\mathrm{Re}_p = \mathrm{Re}_{PF}$, both modes (three eigenvalues) are neutrally stable, i.e., have eigenvalues with zero real part.

To illustrate the stability of the log-rolling state depending on Re_p and St, the stability of λ_p and λ_f are plotted in Fig. 8. Note the resemblance to the state space in Fig. 3. Decreasing the numerical grid resolution in the LSA, model we arrive at almost identical results, and we can conclude that the results from the LSA model are converged in terms of grid resolution. We also find that the values of St_{TZ} and Re_{PF} from the DNS with higher resolution seem to be approaching the values found in the LSA. We therefore believe that grid resolution is the main reason for the DNS results not matching the LSA. Using the values for $\mathrm{Re}_{LR,\mathrm{St}\approx 0}$, Re_{PF}, and St_{TZ} obtained from the LSA, we can now create a quantitatively accurate version of the simplified topology in Fig. 3(b), with all critical values obtained with accurate methods:

(1) $\mathrm{Re}_{LR,\mathrm{St}\approx 0}$. Obtained through the LSA model by finding the Re_p at St = 1 where $\Re\lambda_p = 0$ and $\Im\lambda_p \neq 0$.

(2) Re_{PF}. Obtained through the LSA model by finding the Re_p where $\lambda_f = 0$.

TABLE III. Accurate critical values for a prolate spheroid of $r_p = 4$ at $\kappa = 0.2$; the numbers in the rightmost column show the values obtained with the low-resolution DNS (cf. Fig. 3).

Quantity	Accurate values	Low-resolution DNS
$\mathrm{Re}_{LR,\mathrm{St}\approx 0}$	27.5 ± 0.5	–
Re_{PF}	93.4 ± 0.1	61.5 ± 0.5
Re_c	138.5 ± 5	90
St_{TZ}	1975 ± 25	2650 ± 50
$\mathrm{St}^*_{0.5}$	313.3	–

(3) St_{TZ}. Obtained through the LSA model by finding the St at $\mathrm{Re}_p = \mathrm{Re}_{PF}$ ($\lambda_f = 0$) where $\Re\lambda_p = 0$ and $\Im\lambda_p \neq 0$.

(4) Re_c. Obtained by finding a zero-torque solution of a stationary particle in the flow gradient plane ($s_z = 0$) as done in Refs. [29,44].

(5) $\mathrm{St}^*_{0.5}$. Obtained through an analytical expression for this number at $\mathrm{Re}_p = 0$ in Eq. (5).

For a prolate spheroid of $r_p = 4$ at $\kappa = 0.2$, these numbers are summarized in Table III, with the value of Re_c taken from Ref. [44] and can be compared with the values obtained using DNS in Fig. 3. Generally, it is seen that the critical Reynolds numbers are underestimated and the critical Stokes numbers are overestimated in the low-resolution DNS.

D. Effect of confinement

So far, we have only considered the flow problem with a constant confinement of $\kappa = 0.2$. Our aim is to provide results in a domain large enough for spatial boundary conditions to be insignificant, and therefore we need to find the influence of confinement. There are two effects of confined geometry. First, the results can be affected by the fact that we have periodic boundary conditions, which means that flow disturbances from the periodic images of the particle can affect the particle itself. Second, the walls can influence the flow field as the fluid velocity there is forced to be equal to the wall velocity. To investigate these effects, we find the values of Re_{PF}, $\mathrm{Re}_{LR,\mathrm{St}\approx 0}$, and St_{TZ} for a particle with $r_p = 4$ for $\kappa = 0.3, 0.2, 0.15, 0.1$, and 0.05. The results are shown in Fig. 9(a) where we make two observations. First, the results show that the transitions covered in this work are not an effect of either the presence of walls or periodic boundary conditions as the values of the critical transitional numbers converge with increased domain size (lower κ). Second, the true domain-size independent results are slightly overestimated by the values found at $\kappa = 0.2$ but converged at $\kappa < 0.1$. Note that

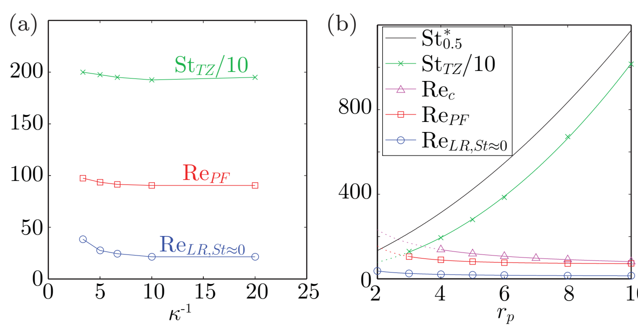

FIG. 9. (a) Critical values of Re_{PF}, $\mathrm{Re}_{LR,\mathrm{St}\approx 0}$, and St_{TZ} at $r_p = 4$ for different values of κ, (b) Critical values Re_{PF}, $\mathrm{Re}_{LR,\mathrm{St}\approx 0}$, $\mathrm{St}^*_{0.5}$, and St_{TZ} for different moderate aspect ratios r_p at $\kappa = 0.05$; the values of Re_c are taken from Ref. [44]; the corresponding empirical relations are described in Table IV.

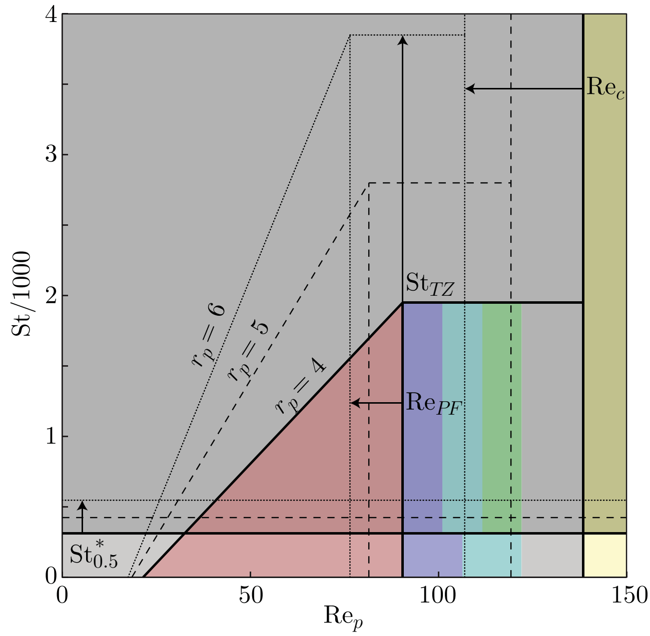

FIG. 10. Simplified topology of the state space using the critical values Re_{PF}, $\mathrm{Re}_{LR,\mathrm{St}\approx 0}$, and St_{TZ} obtained at $\kappa = 0.05$, which are considered converged in terms of domain size; Re_c is taken from Ref. [44] and $\mathrm{St}^*_{0.5}$ taken from Eq. (5); the figure shows the the critical transitions for $r_p = 4$ (solid lines and colored regions), $r_p = 5$ (dashed lines) and $r_p = 6$ (dotted lines) with the arrows indicating how the state space changes with increasing r_p.

the value for Re_c was seen in Ref. [40] to be almost converged at $\kappa = 0.2$. We therefore consider the results of Ref. [44] to be converged in terms of confinement, since these were obtained at $\kappa = 0.2$. The formula of $\mathrm{St}^*_{0.5}$ is, strictly speaking, valid only in an infinite domain ($\kappa = 0$) and $\mathrm{Re}_p = 0$, but was seen in Ref. [29] to be in reasonable agreement with the DNS at $\kappa = 0.2$ and low Re_p.

E. Effect of aspect ratio

Previously we showed the procedure to get an accurate simplified topology of the rotational state space in terms of Re_p and St by using just five critical values: Re_{PF}, $\mathrm{Re}_{LR,\mathrm{St}\approx 0}$, Re_c, $\mathrm{St}^*_{0.5}$, and St_{TZ} [see Fig. 3(b)]. We found the same values for some other moderate aspect ratios, which are illustrated in Fig. 9(b). The values from the LSA (Re_{PF}, $\mathrm{Re}_{LR,\mathrm{St}\approx 0}$, and St_{TZ}) are obtained at $\kappa = 0.05$ and are thus almost fully converged in terms of domain size. The values of Re_c are taken from Ref. [44] and are also considered confinement-independent as described previously. The changes of the critical values due to r_p in the topology of the state space are illustrated in Fig. 10. For the lowest aspect ratio $r_p = 2$, the transition at Re_{PF} is too high ($\mathrm{Re}_{PF} > 150$) and a converged steady state solution of the log-rolling state could not be found in order to perform the LSA. By fitting the data points, we can provide the empirical formulas for the critical values: Re_{PF}, $\mathrm{Re}_{LR,\mathrm{St}\approx 0}$, Re_c, and St_{TZ} in Table IV. Even though the empirical formula of Re_c lacks support for particles with $r_p \lesssim 4$, there are still indications that $\mathrm{St}^*_{0.5} < \mathrm{Re}_c$ at $r_p = 2$. This, in turn, would imply that the nonplanar dynamics can be chaotic even for a neutrally buoyant particle where $\mathrm{St} = \mathrm{Re}_p$, which is exactly what was observed both in Refs. [26,29].

Throughout this study, we have been considering only the case of a prolate spheroid where $r_p > 1$. The case of an oblate spheroid ($r_p < 1$) was extensively studied in Refs. [44,51]. It was found that log rolling was always stable as $\kappa \to 0$ regardless of Re_p or St. Two critical transitions

TABLE IV. Empirical formulas for the critical values Re_{PF}, $\mathrm{Re}_{LR,\mathrm{St}\approx 0}$, Re_c, and St_{TZ} for a prolate spheroid with moderate aspect ratios in simple shear flow; the data used for Re_c are taken at $\kappa = 0.2$ from Ref. [44]; the other formulas are fitted to the data from the LSA analysis at $\kappa = 0.05$.

$\mathrm{Re}_{LR,\mathrm{St}\approx 0} = 72.1 r_p^{-1.5} + 12.6$
$\mathrm{Re}_{PF} = 371.1 r_p^{-2.1} + 69.0$
$\mathrm{Re}_c = 374.6 r_p^{-1.0} + 43.1$
$\mathrm{St}_{TZ} = 95.5 r_p^{2.0} + 401.6$

between rotational states were found. First, the tumbling motion was seen to stabilize for thin oblate particles, which was a transition also dependent on Re_p and St. Second, a steady state was found at $\mathrm{Re}_p > \mathrm{Re}_c$ also for oblate particles. Both these transitions were fully described quantitatively in these works. The data from Rosén *et al.* [44] of Re_c are fitted here with a similar empirical formula as in Table IV:

$$\mathrm{Re}_{c,\mathrm{oblate}} = 367.1 r_p^{2.0} + 5.5. \tag{9}$$

IV. CONCLUSIONS

This work provides a quantitatively accurate description of a prolate spheroid in a simple shear flow at moderate Re_p. Previous direct numerical simulations (DNS) on the same flow problem [24–29,40] have been inconsistent in terms of critical transitional numbers. This is believed to be owing to the problem of resolving the fluid close to the particle boundary. This problem also leads to numerical difficulties to study the true effect of the finite domain size, since very small particles need to be resolved in a huge domain at low κ.

Here we first studied the state space qualitatively with DNS to characterize the important dynamical transitions. This was done at much higher St than previously done by Rosén *et al.* [29], in order to get a complete picture of the state-space as $\mathrm{St} \to \infty$, and we found that five critical values of the governing parameters were sufficient to draw a simplified topology of the state space: Re_{PF}, $\mathrm{Re}_{LR,St\approx 0}$, St_{TZ}, Re_c, and $\mathrm{St}^*_{0.5}$.

We showed that three of these critical values (Re_{PF}, $\mathrm{Re}_{LR,\mathrm{St}\approx 0}$, and St_{TZ}) can be accurately obtained through a linear stability analysis (LSA) of the log-rolling prolate spheroid.

It has previously been shown that the fourth critical value, describing the steady-state transition at $\mathrm{Re}_p = \mathrm{Re}_c$, can be accurately, numerically, predicted by finding a zero-torque solution on a stationary particle [29,44] without the use of a moving grid.

The final critical value $\mathrm{St}^*_{0.5}$ describes when the particle inertial forces are of the same magnitude as the viscous forces from the fluid [31,32] and can be found through analytical expressions at $\mathrm{Re}_p = 0$. Although, the number is derived without any inertia in the fluid, $\mathrm{St}^*_{0.5}$ is seen to be relevant even at higher Re_p and describing when the particle dynamics becomes inertial and dependent on the particle angular acceleration. This can even lead to complicated nonplanar dynamics and chaotic rotational states. The fact that $\mathrm{St}^*_{0.5}$ is low for particles with low r_p shows that the complicated dynamics can be present even for a neutrally buoyant particle, which is exactly what is observed in previous work [26,29].

The combined qualitative and quantitative analysis finally provides us an accurate description of all stable rotational states of a single prolate spheroid in simple shear flow given Re_p, St, and r_p. This state space can also be analyzed in terms of channel confinement without significant increase in computational effort. The LSA method has, furthermore, already been proven in Ref. [44] to be consistent with analytical results in the low Re_p regime.

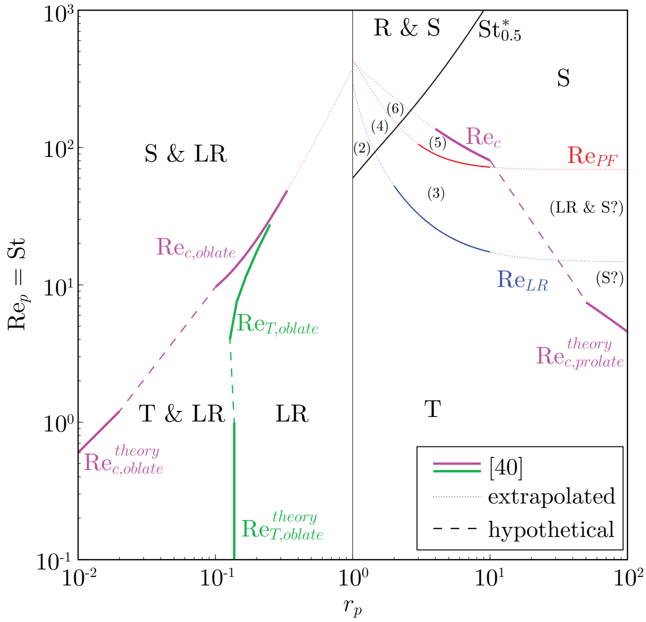

FIG. 11. Rotational states for a neutrally buoyant ($\mathrm{St} = \mathrm{Re}_p$) spheroid depending on Re_p and r_p; T = tumbling; R = rotating; S = steady state; LR = log rolling; the regions (2)–(6) in the upper right part refer to Table II; the theoretical results of $\mathrm{Re}_{c,\mathrm{oblate}}^{\mathrm{theory}}$ and $\mathrm{Re}_{c,\mathrm{prolate}}^{\mathrm{theory}}$ for thin oblate slender prolate spheroids, respectively, as well as the numerical and theoretical values of $\mathrm{Re}_{T,\mathrm{oblate}}$ are taken from Ref. [44]; the dotted lines are the extrapolated values according to the empirical formulas in this work; the dashed lines are only hypothetical to connect numerical results to the theoretical results in Ref. [44].

The present LSA has enabled us to find the true distinction between fluid and particle inertial effects in this flow problem and that this transition is well described by the critical value of $\mathrm{St}_{0.5}^*$. In the absence of particle inertia, at $\mathrm{St} \ll \mathrm{St}_{0.5}^*$, the dynamics of the particle is well described by the two-dimensional noninertial dynamics of the DVP oscillator. This condition of the Stokes number is typically true for all neutrally buoyant prolate spheroids if $r_p \gtrsim 4$. The fact that the infinite dimensional dynamical system of a spheroid in a shear flow can be modeled with a simple two-dimensional system is particularly interesting for the development of a usable model in a LPT framework that can include effects of fluid inertia. Since a two-dimensional DVP oscillator captures the dynamics without any particle inertia, this probably means that there is only a need to modify the torque expressions in Ref. [11] to correctly mimic the effects from moderate fluid inertia. The empirical formulas obtained in Table IV together with results in Refs. [41,42,44] can be used in order to validate such a model.

Combining the present results with the accurate results at low Re_p from Ref. [44], we can now predict the rotational states of neutrally buoyant ($\mathrm{St} = \mathrm{Re}_p$) spheroidal particles at moderate aspect ratios $r_p \in [0.1,0.5]$ (oblate) and $r_p \in [2,10]$ (prolate) at any $\mathrm{Re}_p \in [0,150]$. This is summarized in Fig. 11. Any extrapolations to other r_p and higher Re_p, using the empirical formulas provided in this work are indicative at best. For oblate particles, the numerical results match well with the theory, but it is clear that there is some unknown dynamics still to be explored at $r_p > 10$ since Re_c and $\mathrm{Re}_{c,\mathrm{prolate}}^{\mathrm{theory}}$ do not seem to join into one curve. The empirical relationships suggest that $\mathrm{Re}_c < \mathrm{Re}_{PF}$ at $r_p \gtrsim 13.7$, which would mean that the steady state can coexist with the log-rolling state for such particles. For even more slender prolate spheroids, the theoretical results indicate that $\mathrm{Re}_c < \mathrm{Re}_{LR}$, which would mean that the steady state appears before any of the nonplanar states are stabilized.

These observations however are made based on *the extrapolation* of the present results; thus, it is clear that more studies are needed at $r_p > 10$.

In conclusion, the results from this work can be used for understanding the orientational dynamics in any dilute suspension flow with elongated particles with moderate aspect ratios. Given a local shear rate (and thus Re_p) in the suspension flow, not only can we predict a probable stable orientational distribution, we can also predict the local effective viscosity due to the suspended particles in that region [27,29]. However, careful experiments will be needed in the future to establish the true usefulness of such rheological predictions.

ACKNOWLEDGMENTS

The authors gratefully acknowledge Prof. B. Mehlig, Dr. J. Einarsson, and Dr. C. Ford for their helpful comments and suggestions to this paper. T.R. and F.L. acknowledge financial support from Wallenberg Wood Science Center (WWSC), Bengt Ingeström's Foundation, and ÅForsk (Ångpanneföreningens Foundation for Research and Development). The simulations were performed on resources provided by the Swedish National Infrastructure for Computing (SNIC) at the High Performance Computing Center North (HPC2N) and the National Supercomputer Center (NSC) in Linköping, Sweden.

---

[1] F. Lundell, L. D. Söderberg, and P. H. Alfredsson, Fluid mechanics of papermaking, Annu. Rev. Fluid Mech. **43**, 195 (2011).

[2] L. J. Lanticse, Y. Tanabe, K. Matsui, Y. Kaburagi, K. Suda, M. Hoteida, M. Endo, and E. Yasuda, Shear-induced preferential alignment of carbon nanotubes resulted in anisotropic electrical conductivity of polymer composites, Carbon **44**, 3078 (2006).

[3] Z. Li, J. Zhu, and C. Zhang, Numerical simulations of ultrafine powder coating systems, Powder Tech. **150**, 155 (2005).

[4] Marcos, J. R. Seymour, M. Luhar, W. M. Durham, J. G. Mitchell, A. Macke, and R. Stocker, Microbial alignment in flow changes ocean light climate, Proc. Natl. Acad. Sci. USA **108**, 3860 (2011).

[5] D. A. Reasor, M. Mehrabadi, D. N. Ku, and C. K. Aidun, Determination of critical parameters in platelet margination, Ann. Biomed. Eng. **41**, 238 (2013).

[6] H. L. Pésceli, J. Trulsen, and Ø. Fiksen, Predator-prey encounter and capture rates for plankton in turbulent environments, Prog. Oceanogr. **101**, 14 (2012).

[7] A. Stohl, A. J. Prata, S. Eckhardt, L. Clarisse, A. Durant, S. Henne, N. L. Kristiansen, A. Minikin, U. Schumann, P. Seibert, K. Stebel, H. E. Thomas, T. Thorsteinsson, K. Tørseth, and B. Weinzierl, Determination of time- and height-resolved volcanic ash emissions and their use for quantitative ash dispersion modeling: the 2010 Eyjafjallajökull eruption, Atmos. Chem. Phys. **11**, 4333 (2011).

[8] G. Ventura, R. De Rosa, E. Colletta, and R. Mazzuoli, Deformation patterns in a high-viscosity lava flow inferred from the crystal preferred orientation and imbrication structures: an example from Salina (Aeolian Islands, southern Tyrrhenian Sea, Italy), Bull. Volcanol. **57**, 555 (1996).

[9] G. Falkovich, A. Fouxon, and M. G. Stepanov, Acceleration of rain initiation by cloud turbulence, Nature (London) **419**, 151 (2002).

[10] C. T. Crowe, J. D. Schwarzkopf, M. Sommerfeld, and Y. Tsuji, *Multiphase Flows with Droplets and Particles*, 2nd ed. (CRC Press, Boca Raton, FL, 2012).

[11] G. B. Jeffery, The motion of ellipsoidal particles immersed in a viscous fluid, Proc. R. Soc. Lond. A **102**, 161 (1922).

[12] R. C. Givler, M. J. Crochet, and R. B. Pipes, Numerical prediction of fiber orientation in dilute suspensions, J. Compos. Mater. **17**, 330 (1983).

[13] C. Marchioli, M. Fantoni, and A. Soldati, Orientation, distribution, and deposition of elongated, inertial fibers in turbulent channel flow, Phys. Fluids **22**, 033301 (2010).

[14] N. R. Challabotla, L. Zhao, and H. I. Andersson, Orientation and rotation of inertial disk particles in wall turbulence, J. Fluid. Mech. **766**, R2 (2015).

[15] K. Gustavsson, J. Einarsson, and B. Mehlig, Tumbling of Small Axisymmetric Particles in Random and Turbulent Flows, Phys. Rev. Lett. **112**, 014501 (2014).

[16] E-J. Ding and C. K. Aidun, The dynamics and scaling law for particles suspended in shear flow with inertia, J. Fluid. Mech. **423**, 317 (2000).

[17] C. M. Zettner and M. Yoda, The circular cylinder in simple shear at moderate Reynolds numbers: An experimental study, Exp. Fluids **30**, 346 (2001).

[18] C. M. Zettner and M. Yoda, Moderate aspect ratio elliptical cylinders in simple shear with inertia, J. Fluid. Mech. **442**, 241 (2001).

[19] M. R. Maxey and J. J Riley, Equation of motion for a small rigid sphere in a nonuniform flow, Phys. Fluids **26**, 883 (1983).

[20] E. Balkovsky, G. Falkovich, and A. Fouxon, Intermittent Distribution of Inertial Particles in Turbulent Flows, Phys. Rev. Lett. **86**, 2790 (2001).

[21] A. L. Yarin, O. Gottlieb, and I. V. Roisman, Chaotic rotation of triaxial ellipsoids in simple shear flow, J. Fluid. Mech. **340**, 83 (1997).

[22] F. Lundell, The effect of particle inertia on triaxial ellipsoids in creeping shear: From drift toward chaos to a single periodic solution, Phys. Fluids **23**, 011704 (2011).

[23] J. Einarsson, B. M. Mihiretie, A Laas, S Ankardal, J. R. Angilella, D. Hanstorp, and B. Mehlig, Tumbling of asymmetric microrods in a microchannel flow, Phys. Fluids **28**, 013302 (2016).

[24] D. Qi and L.-S. Luo, Rotational and orientational behavior of three-dimensional spheroidal particles in Couette flows, J. Fluid. Mech. **477**, 201 (2003).

[25] Z. Yu, N. Phan-Thien, and R. I. Tanner, Rotation of a spheroid in a Couette flow at moderate Reynolds numbers, Phys. Rev. E **76**, 026310 (2007).

[26] H. Huang, X. Yang, M. Krafczyk, and X-Y. Lu, Rotation of spheroidal particles in Couette flows, J. Fluid. Mech. **692**, 369 (2012).

[27] H. Huang, Y.-F. Wu, and X.-Y. Lu, Shear viscosity of dilute suspensions of ellipsoidal particles with a lattice Boltzmann method, Phys. Rev. E **86**, 046305 (2012).

[28] W. Mao and A. Alexeev, Motion of spheroid particles in shear flow with inertia, J. Fluid. Mech. **749**, 145 (2014).

[29] T. Rosén, F. Lundell, M. Do-Quang, and C. K. Aidun, The combined effect from fluid and particle inertia on the dynamical states of a prolate spheroidal particle suspended in shear flow, J. Fluid. Mech. **771**, 115 (2015).

[30] F. P. Bretherton, The motion of rigid particles in a shear flow at low Reynolds number, J. Fluid. Mech. **14**, 284 (1962).

[31] F. Lundell and A. Carlsson, Heavy ellipsoids in creeping shear flow: Transitions of the particle rotation rate and orbit shape, Phys. Rev. E **81**, 016323 (2010).

[32] C. Nilsen and H. I. Andersson, Chaotic motion of inertial spheroids in oscillating shear flow, Phys. Fluids **25**, 013303 (2013).

[33] G. I. Taylor, The motion of ellipsoidal particles in a viscous fluid, Proc. R. Soc. Lond. A **103**, 58 (1923).

[34] R. C. Binder, The motion of cylindrical particles in viscous flow, J. Appl. Phys. **10**, 711 (1939).

[35] B. J. Trevelyan and S. G. Mason, Particle motions in sheared suspensions. I. Rotations, J. Coll. Sci., Imp. Univ. Tokyo **6**, 354 (1951).

[36] A. Karnis, H. L. Goldsmith, and S. G. Mason, Axial migration of particles in Poiseuille flow, Nature (London) **200**, 159 (1963).

[37] P. G. Saffman, On the motion of small spheroidal particles in a viscous liquid, J. Fluid. Mech. **1**, 540 (1956).

[38] G. Subramanian and D. L. Koch, Inertial effects on fibre motion in simple shear flow, J. Fluid. Mech. **535**, 383 (2005).

[39] G. Subramanian and D. L. Koch, Inertial effects on the orientation of nearly spherical particles in simple shear flow, J. Fluid. Mech. **557**, 257 (2006).
[40] T. Rosén, F. Lundell, and C. K. Aidun, Effect of fluid inertia on the dynamics and scaling of neutrally buoyant particles in shear flow, J. Fluid. Mech. **738**, 563 (2014).
[41] J. Einarsson, F. Candelier, F. Lundell, J. R. Angilella, and B. Mehlig, Effect of weak fluid inertia upon Jeffery orbits, Phys. Rev. E **91**, 041002 (2015).
[42] J. Einarsson, F. Candelier, F. Lundell, J. R. Angilella, and B. Mehlig, Rotation of a spheroid in a simple shear at small Reynolds number, Phys. Fluids **27**, 063301 (2015).
[43] F. Candelier, J. Einarsson, F. Lundell, B. Mehlig, and J. R. Angilella, Role of inertia for the rotation of a nearly spherical particle in a general linear flow, Phys. Rev. E **91**, 053023 (2015).
[44] T. Rosén, J. Einarsson, A. Nordmark, C. K. Aidun, F. Lundell, and B. Mehlig, Numerical analysis of the angular motion of a neutrally buoyant spheroid in shear flow at small Reynolds numbers, Phys. Rev. E **92**, 063022 (2015).
[45] P. Holmes and D. Rand, Phase portraits and bifurcations of the nonlinear oscillator: $\ddot{x} + (\alpha + \gamma x^2)\dot{x} + \beta x + \delta x^3$, Int. J. Nonlin. Mech. **15**, 449 (1980).
[46] K. R. Schenk-Hoppé, Bifurcation scenarios of the noisy duffing-van der pol oscillator, Nonlinear Dynam. **11**, 255 (1996).
[47] J. Hale and H. Koçak, *Dynamics and Bifurcations, Texts in Applied Mathematics*, Vol. 3 (Springer-Verlag, New York, 1991).
[48] C. K. Aidun and J. R. Clausen, Lattice-Boltzmann method for complex flows, Annu. Rev. Fluid Mech. **42**, 439 (2010).
[49] J. R. Clausen and C. K. Aidun, Galilean invariance in the lattice-Boltzmann method and its effect on the calculation of rheological properties in suspensions, Int. J. Multiphas. Flow **35**, 307 (2009).
[50] J. Wu and C. K. Aidun, Simulating 3D deformable particle suspensions using lattice Boltzmann method with discrete external boundary force, Int. J. Numer. Meth. Fl. **62**, 765 (2010).
[51] T. Rosén, M. Do-Quang, C. K. Aidun, and F. Lundell, Effect of fluid and particle inertia on the rotation of an oblate spheroidal particle suspended in shear flow, Phys. Rev. E **91**, 053017 (2015).
[52] Comsol Multiphysics Reference Manual, version 5.1 (www.comsol.com, 2015).
[53] http://www.caam.rice.edu/software/ARPACK/.
[54] O. Tammisola, F. Lundell, P. Schlatter, A. Wehrfritz, and L. D. Söderberg, Global linear and nonlinear stability of viscous confined plane wakes with co-flow, J. Fluid. Mech. **675**, 397 (2011).